




Article

One-Pot Synthesis of Sulfur-Doped TiO₂/Reduced Graphene Oxide Composite (S-TiO₂/rGO) with Improved Photocatalytic Activity for the Removal of Diclofenac from Water

Marin Kovačić ^{1,*} , Klara Perović ¹, Josipa Papac ¹, Antonija Tomić ¹, Lev Matoh ², Boštjan Žener ², Tomislav Brodar ³, Ivana Capan ³ , Angelja K. Surca ⁴, Hrvoje Kušić ^{1,*}, Urška Lavrenčič Štangar ²  and Ana Lončarić Božić ¹

¹ Faculty of Chemical Engineering and technology, University of Zagreb, Marulićev trg 19, HR-10000 Zagreb, Croatia; kperovic@fkit.hr (K.P.); jpapac@fkit.hr (J.P.); atomic@fkit.hr (A.T.); abozic@fkit.hr (A.L.B.)

² Faculty of Chemistry and Chemical Technology, University of Ljubljana, Večna pot 113, SI-1000 Ljubljana, Slovenia; lev.matoh@fkkt.uni-lj.si (L.M.); bostjan.zener@fkkt.uni-lj.si (B.Ž.); urska.lavrencic.stangar@fkkt.uni-lj.si (U.L.Š.)

³ Division of Material Physics, Ruđer Bošković Institute, Bijenička cesta 54, HR-10000 Zagreb, Croatia; tomislav.brodar@irb.hr (T.B.); ivana.capan@irb.hr (I.C.)

⁴ Department of Chemistry, National Institute of Chemistry, Hajdrihova 19, SI-1001 Ljubljana, Slovenia; angelja.k.surca@ki.si

* Correspondence: mkovacic@fkit.hr (M.K.); hkusic@fkit.hr (H.K.); Tel.: +385-1-4597-145 (M.K.); +385-1-4597-281 (H.K.)

Received: 3 March 2020; Accepted: 27 March 2020; Published: 1 April 2020



Abstract: Sulfur-doped TiO₂ (S-TiO₂) composites with reduced graphene oxide (rGO), wt. % of rGO equal to 0.5%, 2.75%, and 5.0%, were prepared by a one-pot solvothermal procedure. The aim was to improve photocatalytic performance in comparison to TiO₂ under simulated solar irradiation for the treatment of diclofenac (DCF) in aqueous medium. The obtained composites were characterized for physical-chemical properties using thermogravimetric analysis (TGA), X-ray diffractograms (XRD), Raman, scanning electron microscopy (SEM)/energy dispersive X-ray (EDX), Brauner Emmett Teller (BET), and photoluminescence (PL) analyses, indicating successful sulfur doping and inclusion of rGO. Sulfur doping and rGO have successfully led to a decrease in photogenerated charge recombination. However, both antagonistic and synergistic effects toward DCF treatment were observed, with the latter being brought forward by higher wt.% rGO. The composite with 5.0 wt.% rGO has shown the highest DCF conversion at pH 4 compared to that obtained by pristine TiO₂, despite lower DCF adsorption during the initial dark period. The expected positive effects of both sulfur doping and rGO on charge recombination were found to be limited because of the subpar interphase contact with the composite and incomplete reduction of the GO precursor. Consequent unfavorable interactions between rGO and DCF negatively influenced the activity of the studied S-TiO₂/rGO photocatalyst under simulated solar irradiation.

Keywords: solar photocatalysis; sulfur-doped TiO₂; TiO₂-reduced graphene oxide composite; diclofenac

1. Introduction

The prospects of TiO₂ photocatalysis are immense, ranging from clean energy production to water purification using solar irradiation [1,2]. However, the activity of pristine TiO₂ under solar

irradiation of is hindered by low absorption within the visible spectrum, because of its prohibitively wide bandgap. Second, the performance of TiO_2 in those cases is likewise hindered by photogenerated charge recombination. Some studies have shown that up to 90% of the photogenerated charges recombine, releasing heat as a byproduct, and hence do not perform useful photocatalytic work [3]. Hence, suppression of charge recombination would further yield an improvement in photocatalytic activity for the processes of interest. Improvements with respect to higher photocatalytic activity under visible irradiation can be achieved by: (i) Deposition of noble metals on the surface of TiO_2 , (ii) doping the crystalline lattice of TiO_2 , (iii) creating composites with other semiconducting materials, and (iv) with dye-sensitizers, providing transfer of the photogenerated electron from or to TiO_2 [4–7]. An attractive solution is the implementation of graphene or reduced graphene oxide (rGO) as an electron sink, akin to the function of deposited noble metals, but at a significantly lower cost. High conductivity of graphene and reduced graphene oxide (rGO) facilitates electron transfer, providing decreased recombination rates [8]. Furthermore, rGO can promote photocatalytic activity toward degradation by adsorbing pollutants, thereby increasing the odds of the reaction occurring between the adsorbed pollutant and surface-generated radical species [9]. Graphene oxide (GO) can be reduced using harmful reducing agents or benign agents, such as green tea extract [10,11]. TiO_2 /rGO composites can be prepared by sol-gel and solvothermal procedures with simultaneous TiO_2 growth and GO reduction to rGO, colloidal blending and ionothermal methods [12–15]. Sulfur doping can significantly decrease the band gap of TiO_2 and can promote the inhibition of photogenerated charge recombination, thereby improving photocatalytic activity under solar irradiation. Sulfur doping of TiO_2 can be achieved by sol-gel, hydrothermal and coprecipitation syntheses [16–20]. In this paper, a sulfur-doped TiO_2 (S- TiO_2) and rGO composite with varying wt. % of rGO was obtained in a one-pot solvothermal synthesis. The simultaneous reduction and doping were achieved by in situ generated sulfide ions (S^{2-}) from thioacetamide hydrolysis under solvothermal conditions. The photocatalytic performance of immobilized S- TiO_2 /rGO thin films for DCF abatement in water under simulated solar irradiation was investigated.

2. Materials and Methods

2.1. Preparation of Graphene Oxide (GO)

All chemicals used in this work were of analytical or higher grade. Graphene oxide (GO) was prepared according to the Hummers procedure with minor modifications [21]. Graphite flakes (C, Sigma-Aldrich) were ground and sieved. Total of 3 g of mesh 70 graphite was treated with 69 mL of sulfuric acid (H_2SO_4 , Honeywell) and 1.5 g of dry sodium nitrate (NaNO_3 , Kemika) in an ice bath. Total of 9 g of potassium permanganate (KMnO_4 , Kemika) was added to the mixture, taking care not to rise the temperature significantly. After 1 h of stirring, demineralized water was slowly added until the temperature reached near boiling. The mixture was then allowed to cool and was subsequently diluted with 1 L of deionized water. Hydrogen peroxide (H_2O_2 , 30%, T.T.T.) was added to the diluted solution, until the cessation of the observed effervescence. The mixture was centrifuged, and the whitish precipitate was discarded, while the brownish floating product was rinsed with 5% hydrochloric acid (HCl, Kemika). The residual acid was washed until the suspension became nearly pH neutral. The suspension was dialyzed for 14 d with a Spectrum chemical Spectra/Por membrane in ultrapure water. Water from the obtained suspension was removed in vacuum at 35 °C.

2.2. Solvothermal Synthesis of TiO_2 and S- TiO_2 Reduced Graphene Oxide Composite (S- TiO_2 /rGO)

GO obtained from the previous procedure was added to 96% ethanol ($\text{CH}_3\text{CH}_2\text{OH}$, EtOH, Gram-mol) in order to obtain a suspension of $\gamma(\text{GO}) = 1 \text{ mg mL}^{-1}$ and was subsequently sonicated for 30 min using a Cole Parmer EW-08848 ultrasonic bath (Cole Parmer, Vernon Hills, IL, USA). An appropriate aliquot of the resulting GO/EtOH suspension needed to achieve the resulting 0.5, 2.75, and 5.0 wt.% of the reduced graphene oxide (rGO) was transferred to a 50 mL polytetrafluoroethylene

(PTFE) reactor. Afterwards 200 mg \pm 5 mg of thioacetamide (CH_3SNH_2 , TAA, Acros Organics) was added under constant stirring, along with 1 mL of glacial acetic acid (CH_3COOH , Fluka). Upon dissolution of thioacetamide, a 1 mL aliquot of tetrabutyl orthotitanate ($\text{Ti}(\text{OCH}_2\text{CH}_2\text{CH}_2\text{CH}_3)_4$, TBT, Acros Organics) was added under stirring. In order to obtain pristine TiO_2 , GO and thioacetamide were omitted from the synthesis. The PTFE reactor was transferred to a stainless steel autoclave and heated to 180 °C for 12 h in a UN-55 laboratory oven (Mettler, Schwabach, Germany). After cooling to room temperature, the product was centrifuged and rinsed successively three times with distilled water. The product slurry was then dried at 60 °C under vacuum.

2.3. Immobilization of S-TiO₂/rGO Composites

The obtained composite was immobilized on round glass substrates ($r = 37.5$ mm) using a low-temperature procedure developed by Kete et al. [22]. The procedure calls for the preparation of a titania precursor sol and silica precursor sol. The titania sol was obtained by perchloric acid (HClO_4 , Kemika) catalyzed hydrolysis of an ethanolic solution of titanium isopropoxide ($\text{Ti}(\text{OCH}(\text{CH}_3)_2)_4$, Acros Organics) under reflux for 48 h. The silica sol was prepared by hydrochloric acid-catalyzed hydrolysis of tetraethyl orthosilicate ($\text{Si}(\text{OC}_2\text{H}_5)_4$) in water. Once a clear silica sol was obtained, it was mixed with the titania sol, ethanol, and colloidal silica Levasil 200/30 (Obermeier) to form the binder sol. To the binder sol an appropriate amount of S-TiO₂/rGO was added and homogenized in an ultrasonic bath for 15 min. The photocatalyst was deposited on glass substrates by spin coating at 1500 rpm for 30 s using a KW-4A spin coater (Chemat Technology). The plates were finally thermally treated at 200 °C in air for 2 h, using an UN-55 programmable laboratory oven (Mettler, Schwabach, Germany).

2.4. Characterization of the S-TiO₂/rGO Composite

Thermogravimetric analysis (TGA) was performed by heating 5 mg of the sample in a Pt pan, within a temperature range of 25 °C to 600 °C at a heating rate of 10 °C min^{-1} in synthetic air. The analysis was performed on a Q500 TGA analyzer (TA Instruments, New Castle, PA, USA).

Morphological features were determined by scanning electron microscopy (SEM) and energy dispersive X-ray (EDX) spectroscopy, using an Ultra Plus SEM (Zeiss, Jena, Germany) equipped with an Oxford X-Max silicon drift detector. The samples were loaded on a graphite adhesive tape, without vapor phase deposition pretreatment.

Brauner Emmett Teller (BET) specific surface area was determined by N_2 adsorption/desorption isotherms on a Gemini 2380 instrument (Micrometrics, Norcross, GA, USA). The samples were degassed beforehand at 250 °C in vacuum.

X-ray diffractograms (XRD) of the samples were measured with a X'Pert PRO MPD instrument (PANalytical, Almelo, Netherlands), using $\text{Cu K}\alpha_1$ radiation at 2θ from 10° to 70° in 0.033° increments. An ICDD PDF standard card no. 21-1272 was used as anatase reference. D-spacing was calculated according to Equation (1):

$$\frac{1}{d^2} = \frac{h^2 + k^2}{a^2} + \frac{l^2}{c^2} \quad (1)$$

where d represents the interplanar distance, i.e. D-spacing, h , k and l are Miller indices. The size of crystallites was calculated according to the Scherrer Equation (2) [23,24]:

$$\tau = \frac{K\lambda}{\beta \cos \theta} \quad (2)$$

where τ represents the calculated crystallite size, K is a dimensionless factor related to the shape of crystallites ($K = 0.9$), β is the peak width at full maximum (in radians), and θ is the Bragg angle.

Raman spectroscopy was performed on powder samples, using an Alpha300 (Witec, Ulm, Germany) equipped with a microscope and attached atomic force microscope (AFM). A 532 nm laser was used as the excitation source. The integration time was set to 0.5 s, with an average of 100 scans taken.

Photoluminescence (PL) spectra were recorded using a LDM405 405 nm laser diode module (Thorlabs, Newton, NJ, USA) as an excitation source. The emitted PL light was analyzed by a BRC112E CCD array spectrometer (B&W Tek, Newark, NJ, USA).

Diffuse reflectance spectra (DRS) were measured on immobilized thin films by a Lambda 950 UV/Vis spectrometer (Perkin Elmer, Palm Springs, CA, USA), equipped with an integrating sphere. The spectra were recorded at a scan speed of 2063 nm min^{-1} , from 2500 nm to 250 nm. The obtained spectra were transformed into the Kubelka–Munk function vs. photon energy in order to obtain band gap values [25].

2.5. Investigation of Photocatalytic Activity

Photocatalytic experiments for the degradation of 0.1 mM diclofenac sodium ($\text{C}_{14}\text{H}_{11}\text{Cl}_2\text{NO}_2\text{Na}$, DCF, Sigma Aldrich) in water were carried out in a water-cooled batch photoreactor, with the photocatalyst-coated glass plates placed on the bottom of the reactor. The experiments were performed in triplicates. A solar simulator, using a model 69920 power supply, Newport 66921 arc lamp housing fitted with an Osram 450W Xenon arc lamp, and an AM 1.5 G airmass filter (Newport, Irvine, CA, USA) was used to irradiate the photoreactor by a perpendicular, collimated beam of light. A DOS-20 shaker (NeoLab, Heidelberg, Germany) was used to provide mixing within the reactor during the experiments. The pH of the DCF solution was adjusted to 4 ± 0.05 , 6 ± 0.05 , and 8 ± 0.05 in separate experiments, using dilute HCl and NaOH, before quantitatively transferring 90 mL of the solution into the photoreactor. An initial period of 30 min in the dark was provided to achieve adsorption equilibrium of DCF on the immobilized photocatalyst. After initial pH adjustment and achieving equilibrium in the dark, 1.5 mL of the sample was withdrawn from the reactor and filtered through $0.45 \mu\text{m}$ syringe filters into vials for high performance liquid chromatographic (HPLC) analysis. Desorption of DCF from the used plates was performed by immersion in an alkaline solution maintained at pH 8 for half an hour, after which the sample was submitted for HPLC analysis. DCF was detected at a wavelength of 276 nm, using isocratic elution with methanol (CH_3OH , J.T. Baker): 0.1 % formic acid (HCOOH , Fluka) in water = 70:30, on a Nucleosil RP C18 250 mm \times 4.6 mm column (Macherey Nagel, Dueren, Germany). The HPLC used was a LC-20 series (Shimadzu, Kyoto, Japan), equipped with a SPD-M20A UV/DAD detector. All stock solutions were prepared from ultrapure water obtained from a Millipore Direct Q3 UV (Merck EMD, Darmstadt, Germany).

3. Results and Discussion

3.1. Composition and Morphology of the S-TiO₂/rGO Composite

The thermogravimetric curve of the 5% wt.(rGO) composite shown in Figure 1 indicates an unremarkable composition. The mass loss up to 150 °C occurred because of evaporation of adsorbed water, amounting to 2.7% of the initial sample mass. Within the 150 °C to 450 °C interval, a loss of crystalline water and organic residue occurs, amounting to 3.8% of the initial mass. Finally, the onset of rGO oxidation at 450 °C amounts to 4.3% of the initial sample mass, indicating successful inclusion of the rGO within the composite.

In order to gain further insight of rGO occurrence within the titania matrix, a Raman spectrum analysis of the sample was carried out; results are presented in Figure 2.

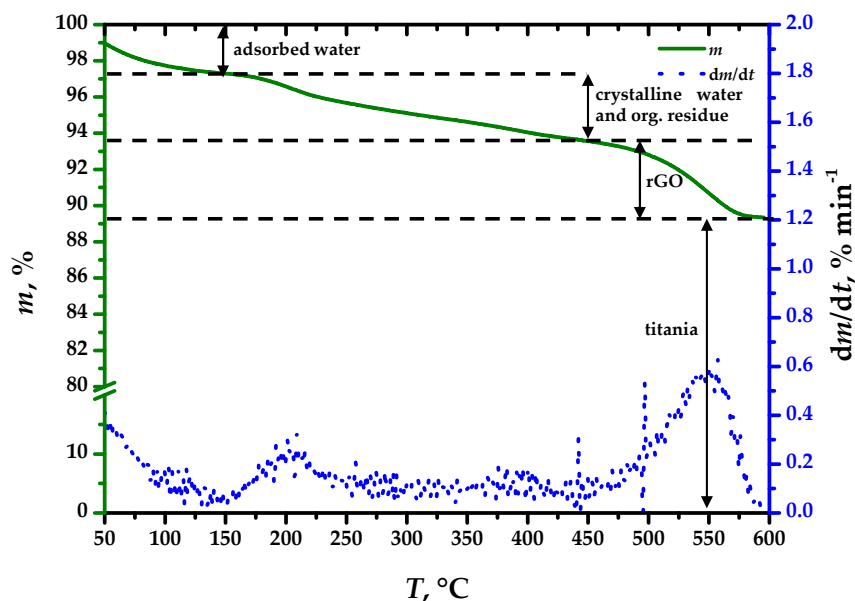


Figure 1. Thermogravimetric analysis of the S-TiO₂/rGO(5.0%) composite.

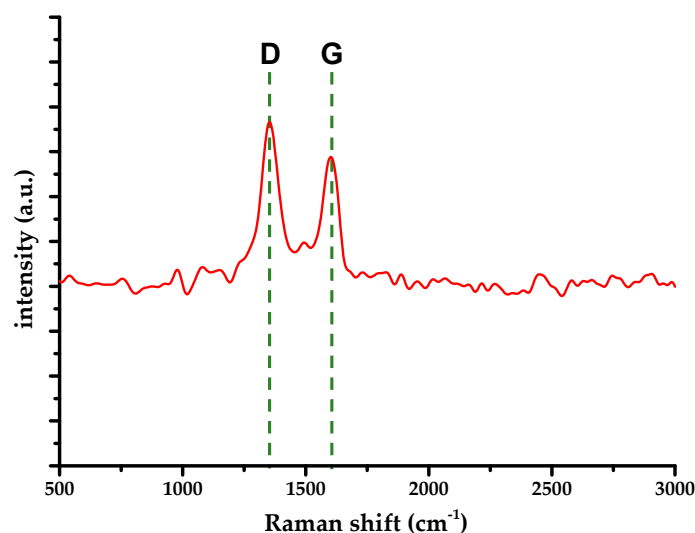


Figure 2. Raman spectrum of S-TiO₂/rGO(5.0%) composite.

The D-mode appears at 1352 cm^{-1} , whereas the G-mode occurs at 1600 cm^{-1} . The G-mode blueshift indicates the presence of residual functional groups, i.e., incomplete reduction of the starting material [26,27]. Those are presumably carbonyl and carboxyl groups that require C-C bond rupture. Furthermore, a ratio of D-mode and G-mode Raman intensities (I_d/I_g) of about 1.4 was calculated, indicating a relatively large number of defects within rGO, supported by the lack of the 2D-mode and relatively wide G-mode peak. Characteristic Raman modes for anatase have not been detected, i.e., they were not discernable because of the noise floor.

The composite appears in the scanning electron micrographs, shown in Figure 3a, as irregular agglomerates, ranging in size from a few micrometers up to several tens of micrometers along the longest dimension. The formation of agglomerates is a consequence of the drying process and subsequent grinding with a pestle and mortar. Upon closer inspection, it can be seen that the S-TiO₂/rGO(5.0%) sample is composed of nanosized TiO₂ particles, into which rGO sheets are sandwiched, as shown in Figure 3b. Such morphology can be considered subpar, as phase contact, and hence charge transfer is limited to the near vicinity of the rGO sheets. However, such phase transfer limitations have been noted by other authors applying similar synthesis procedures of the composites [28].

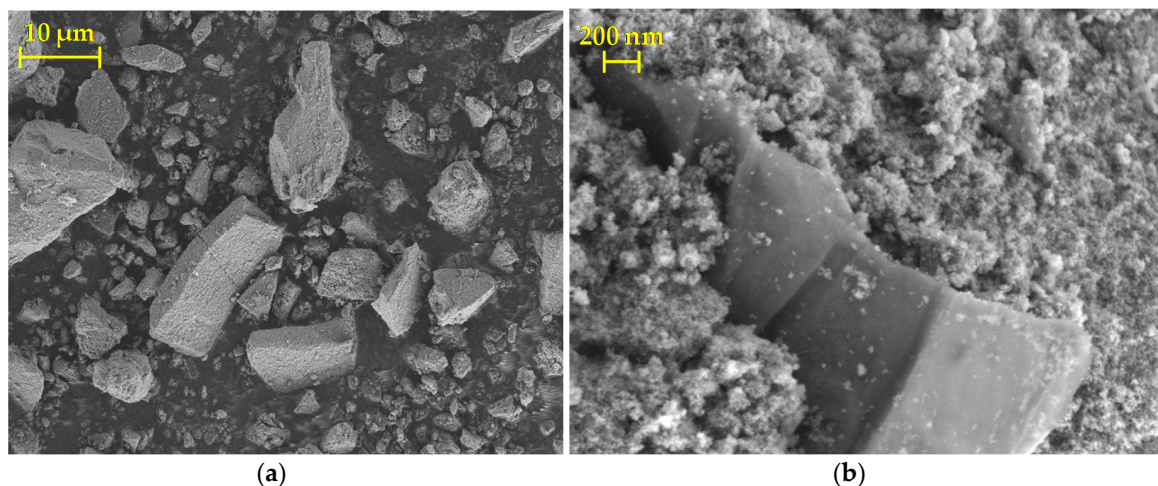


Figure 3. Scanning electron microscopy (SEM) micrographs depicting: (a) S-TiO₂/rGO(5.0%) agglomerates; (b) rGO sandwiched in S-TiO₂ matrix.

The EDX spectrum, shown in Figure 4, in conjunction with XRD, indicates sulfur doping of TiO₂ by nano-sulfur formed by reduction of GO with sulfide as a result of TAA hydrolysis.

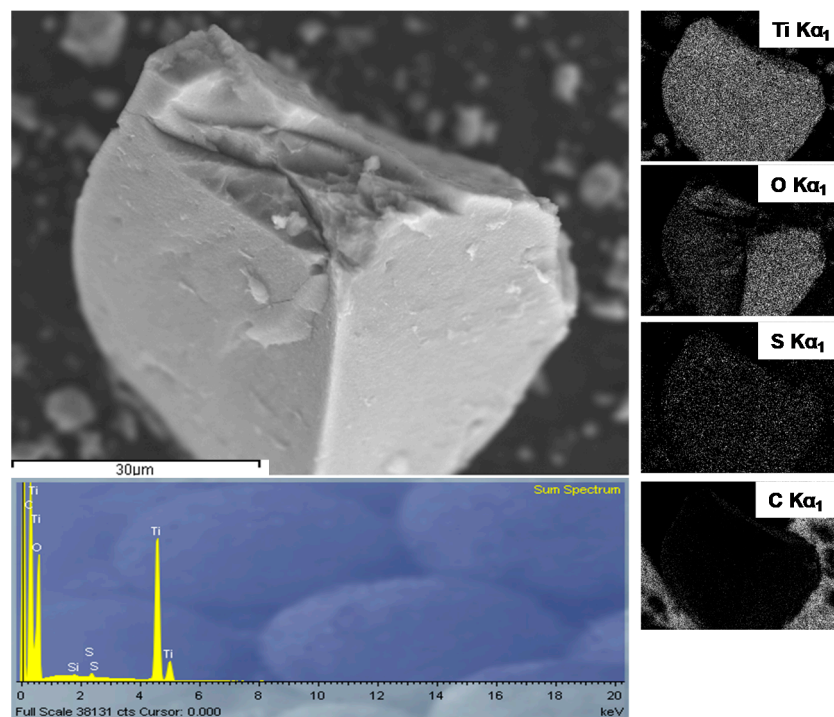


Figure 4. Energy dispersive X-ray (EDX) analysis of S-TiO₂/rGO(5.0%).

Emission of characteristic X-rays display a uniform distribution of sulfur, along with titanium and oxygen, within the sample. The X-ray diffractogram of the S-TiO₂/rGO composite with 5% wt.(rGO), presented in Figure 5, shows a qualitatively lesser degree of crystallinity of anatase phase, in comparison to the diffractogram of pristine TiO₂, as well as a shift in peak positions, indicating lattice defects caused by the inclusion of sulfur. The qualitative decrease of crystallinity is notable from the deterioration of the peaks in the S-TiO₂/rGO (5.0%) diffractogram, i.e., the intensity of the 101 *hkl* index peak decreased and the peak has broadened, while the peaks of 103, 112, 105, and 211 *hkl* indices are hardly discernable.

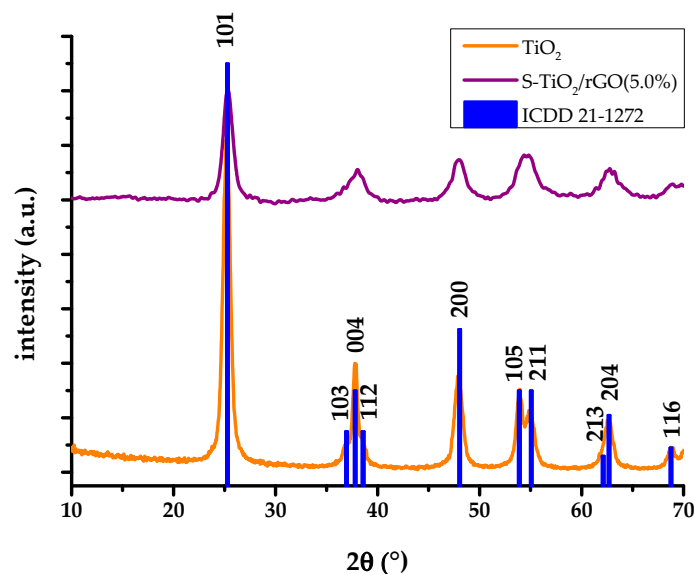


Figure 5. X-ray diffractograms (XRD) analysis of hydrothermally obtained TiO₂ and S-TiO₂/rGO(5.0%).

Calculated lattice parameters, cell volume, and crystallite sizes for TiO₂ and S-TiO₂/rGO(5.0%) are provided in Table 1.

Table 1. Comparison of lattice parameters, d-spacings, cell volumes, and crystallite sizes for TiO₂ and S-TiO₂/rGO (5.0%).

Sample	<i>a</i> , Å	<i>c</i> , Å	<i>d</i> ₁₀₁ , Å	<i>d</i> ₀₀₄ , Å	<i>d</i> ₂₀₀ , Å	Cell Volume, Å ³	<i>τ</i> , nm
TiO ₂	3.798	9.515	3.531	2.379	1.899	137.26	17.5
S-TiO ₂ /rGO(5.0%)	3.787	9.454	3.516	2.363	1.894	135.56	13.4

The results indicate a decrease in cell parameters, and consequently cell volume, because of sulfur doping and the presence of rGO. However, taking into consideration the larger ionic radius of sulfur in comparison to oxygen, such a result is not self-explanatory. Cravanzola et al. [29] studied the effect of sulfur doping on TiO₂ and concluded that sulfur has exchanged oxygen at the surface of TiO₂. Gomathi Devi and Kavitha studied the incorporation of S⁶⁺ into the anatase lattice at Ti⁴⁺ sites and the subsequent contraction of the cell volume [20]. The overall smaller crystallite domains in S-TiO₂/rGO (5.0%) are not small enough to cause a blue-shift in the band gap, because of the quantum confinement, which would negatively affect the activity [30]. The effect of the rGO precursor on the crystallinity of anatase is miniscule and could not be detected in the XRD itself, as supported by the literature findings [28,31].

Photoluminescence spectra, shown on Figure 6, indicate a positive, synergistic effect on the inhibition of charge recombination by sulfur doping and the inclusion of rGO within the TiO₂ matrix, despite relatively poor interphase contact.

The photoluminescence spectrum of TiO₂ shows a typical peak centered at 531 nm, corresponding to the recombination of the conduction band electron and trapped hole or electron quenching by surface adsorbed oxygen [32]. The inclusion of sulfur doping and rGO has resulted in a remarkable decrease of emission, indicating successful inhibition of recombination. Sulfur doping at shallow impurity levels can trap photo-generated charges, according to Liu et al. [33], which is further contributed by rGO acting as an electron-sink. However, the amount of rGO seems to be the key, as the intensity of measured photoluminescence decreased with the increasing amount of rGO within the S-TiO₂/rGO composite. However, increasing rGO wt. % from 2.75% to 5% brings diminishing returns. Higher wt. % of rGO leads to an opposite effect, i.e., an increase in recombination, as rGO can behave as a recombination center [8].

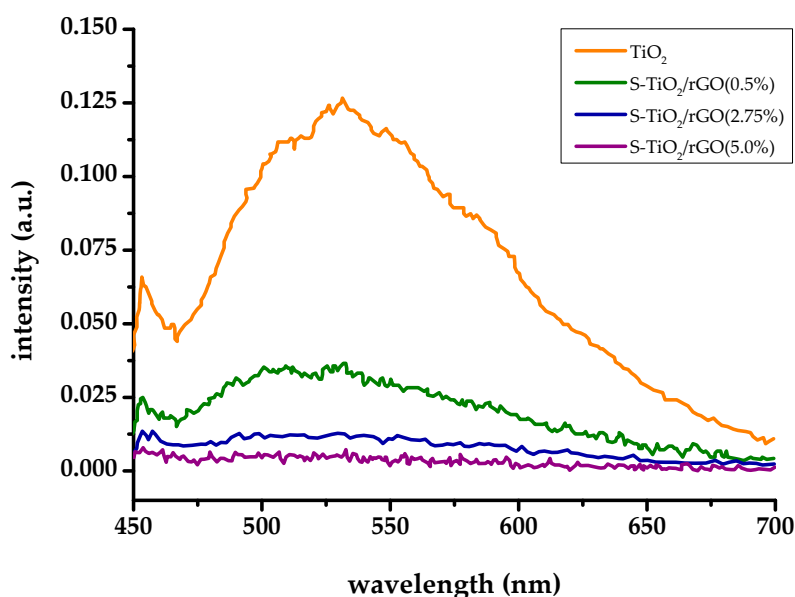


Figure 6. Photoluminescence (PL) spectra of TiO_2 and S- TiO_2/rGO composites.

A further improvement in optoelectronic properties was also noted by DRS, as shown by the Kubelka-Munk transformation of the collected reflectance spectra in Figure 7.

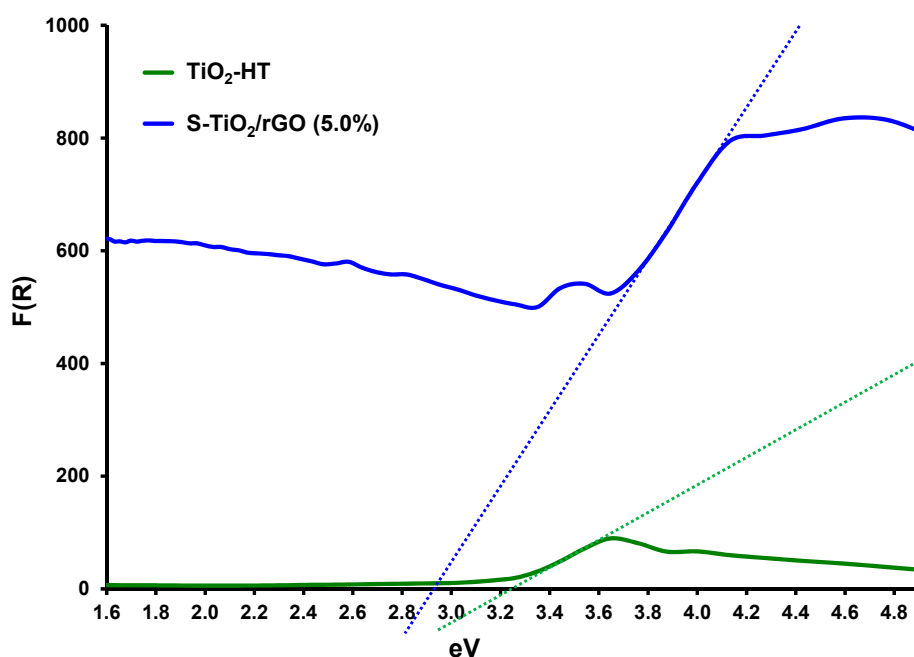


Figure 7. Diffuse reflectance spectra (DRS) spectrum of TiO_2 [34] and S- $\text{TiO}_2/\text{rGO}(5.0\%)$.

The band gap (E_g) of the TiO_2 sample was determined to be 3.21 eV, whereas the band gap for the S- TiO_2/rGO sample was 2.92 eV. The observed reduction in the band gap is a result of sulfur doping and rGO inclusion. Since the recorded spectra did not differ significantly because of the varying rGO content, they were omitted from Figure 7. Literature findings support the hypothesis that varying rGO content in TiO_2 -based photocatalytic materials does not have a discernible effect on lowering of the bandgap [35,36]. Furthermore, Wang et al. [37] found a similar band gap for sulfur-doped TiO_2 , hence sulfur doping and rGO achieve the same band gap narrowing threshold.

Table 2 shows the BET surface areas of TiO_2 , S- TiO_2/rGO composites, and rGO.

Table 2. Surface areas of TiO₂ and S-TiO₂/rGO composites determined by Brauner Emmett Teller (BET) analysis, with pristine TiO₂ being denoted as $w(\text{rGO}) = 0\%$ and rGO with $w(\text{rGO}) = 100\%$.

$w(\text{rGO}), \%$	BET Surface Area, $\text{m}^2 \text{g}^{-1}$
0.0	128.4 ± 1.9 [38]
0.5	123.2 ± 1.6
2.75	128.9 ± 1.4
5.0	131.9 ± 1.8
100.0	17.1 ± 0.19

The obtained results are comparable to the literature findings, based on similar syntheses and drying procedures for TiO₂ and rGO respectively [39,40].

The composite with 0.5 wt.% rGO has a lower surface area than pristine TiO₂, which is to be expected considering the nearly eight-fold difference in specific surface areas of the synthesized TiO₂ and rGO respectively. However, the composite with 2.75 wt.% rGO has a nearly equal surface area to pristine TiO₂ and an increase in surface area with 5.0 wt.% rGO in the composite was observed. Such a contribution can be plausibly attributed to the interaction between TiO₂ and the two-dimensional matt structure of rGO [41].

3.2. Photocatalytic Performance of S-TiO₂/rGO

Photocatalytic effectiveness of the S-TiO₂/rGO composites, in comparison to pristine TiO₂, for the degradation of DCF are compared in Figure 8. Generally, a decrease in removal of DCF, in comparison to TiO₂, can be noted across all experiments with the S-TiO₂/rGO composite. The observed effect is pronounced at pH 6 and 8. First, in the case of the 0.5% wt. rGO composite, i.e., S-TiO₂/rGO(0.5%), the decrease can be attributed primarily to a lower specific surface area, in comparison to pristine TiO₂, as shown in Table 2. The surface area of the aforementioned composite is 4.1% lower than pristine TiO₂ and has achieved nearly 5.6% lower DCF removal after treatment. However, in the case of higher wt.% of rGO, the surface area reasoning for the observed effects does not stand true. rGO contains carboxylic groups, resulting in pK_{a1} of about 4.0, similar to pK_a of DCF and pK_{a2} of 6.0 [42]. Hence at pH 4 and less acidic conditions, repulsion interactions likely occur between rGO and DCF, as they both contain the same deprotonated carboxyl group moiety. π - π interactions between rGO and DCF, which could possibly offset such an effect, are presumably limited because of a significant number of defects within the obtained rGO. Hence, rGO has not shown a beneficial effect toward DCF adsorption, which would promote photocatalytic degradation. The effectiveness of the rGO within the prepared composite is thereby hindered two-fold, first by subpar morphology, and second, by the defects in the structure of rGO, diminishing the supposed advantages a graphene-like material should offer.

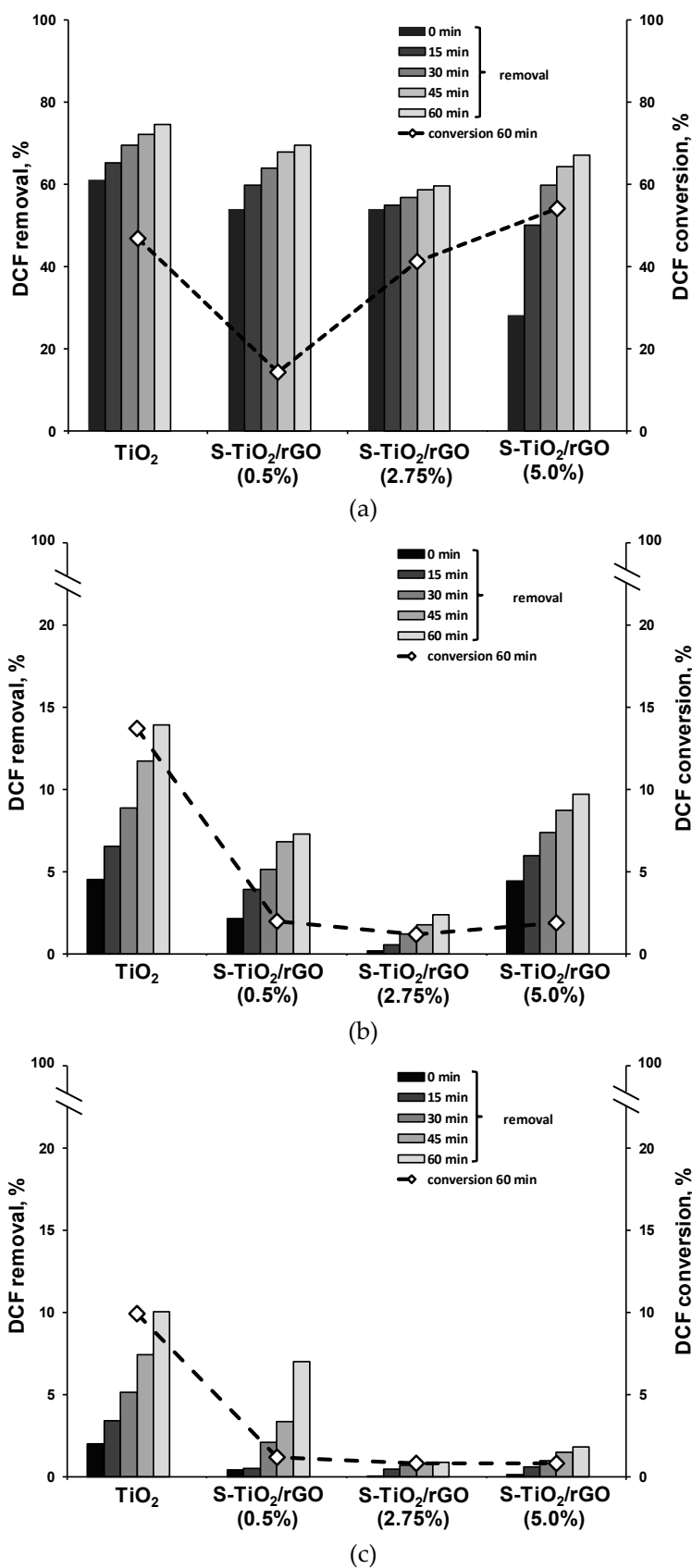


Figure 8. Removal and conversion of diclofenac (DCF) during photocatalytic treatment by solvothermally obtained TiO_2 and $\text{S-TiO}_2/\text{rGO}$ composites at (a) pH 4, (b) pH 6, and (c) pH 8.

The effects of doping TiO₂ with sulfur and combining with rGO are seemingly conflicting in terms of photocatalytic activity. Drastically lower conversion was achieved by the 0.5 wt.% composite, i.e., 14.3% vs. 46.8% achieved by pristine TiO₂ respectively, despite improved inhibition of photo-generated charge recombination in all cases, as previously discussed in terms of PL measurement. Furthermore, the 2.75 wt.% rGO composite has a nearly equal surface area to pristine TiO₂, but has achieved 15.0% less removal after 60 minutes of treatment, whereas initial removal in the dark was on par to 0.5 wt.% rGO. Most probably sulfur-doping, and inclusion of rGO at lower amounts, significantly altered the band edge positions and hence hindered the direct surface degradation of DCF. Increasing wt.% rGO has a markedly positive effect on the conversion of DCF, because of significantly improved recombination inhibition and increased surface area, hence promoting adsorption onto S-TiO₂. The beneficial effect on the composite is even more profound, considering that an increasing amount of rGO in fact lowers the amount of the photocatalytically active component, i.e., TiO₂. At pH 4, the S-TiO₂/rGO 5 wt.% composite achieved 7.33% higher conversion than TiO₂, despite lower adsorption due to unfavorable electrostatic interactions. At pH 6 and pH 8, the surface of the composite S-TiO₂/rGO photocatalyst is negatively charged, resulting in a significant decrease in DCF removal and consequent conversion. It is to be expected, that a shift to a sandwich type composite could yield markedly improved activity, as the phase transfer should be significantly better, therefore improving photogenerated charge separation. Furthermore, the usage of a more pristine graphene-like material should be investigated, in order to assess the impact of incomplete reduction and structural defects.

4. Conclusions

The one-pot simultaneous solvothermal reduction of GO to rGO and production of TiO₂ yielded agglomerates of TiO₂ with sandwiched rGO sheets. EDX analysis indicated effective doping of TiO₂ with sulfur, a product of GO reduction by sulfide ions. The obtained morphology can be considered subpar, as the interphase contact between rGO and TiO₂ does not result in effective photogenerated charge separation. The photocatalytic activity of S-TiO₂/rGO composite for DCF removal and conversion strongly depends on the wt.% of rGO. The 5 wt. % rGO showed improved photocatalytic activity, i.e., conversion in comparison to the benchmark TiO₂, despite a lower removal during the initial dark period. The improved activity can be attributed to effective photogenerated charge separation, as measured by a decrease in PL. Whereas the composite with 0.5 wt. % showed significantly worse activity. rGO has shown to have an antagonistic effect on DCF adsorption due to the incomplete reduction, yielding carboxylic and carbonyl groups that repel DCF. The photocatalytic activity is further hindered by the morphology of the composite, which limits the positive effects of charge transfer between TiO₂ and rGO. At lower wt. % of rGO, the photocatalytic activity is also most likely hindered because of a shift in the band edge position, thus limiting the direct degradation of DCF on the photocatalyst's surface.

Author Contributions: Conceptualization, M.K. and H.K.; data curation, A.L.B., H.K.; formal analysis, M.K. and H.K.; funding acquisition, H.K.; investigation, M.K., K.P., J.P., A.T., L.M., B.Ž., T.B., I.C., and A.K.S.; methodology, M.K., L.M., B.Ž., I.C., and A.K.S.; project administration, H.K.; resources, H.K., U.L.Š.; supervision, H.K., A.L.B.; visualization, M.K., H.K.; writing—original draft preparation, M.K., H.K.; writing—review and editing, H.K., U.L.Š. and A.L.B. All authors have read and agreed to the published version of the manuscript.

Funding: This research was funded by the Croatian Science Foundation, grant number IP-2018-01-1982 (Nano-sized Solar-active Catalysts for Environmental Technologies, NaSCEnT), European Structural and Investment Funds, grant number KK.01.1.1.04.0001 (Water Purification and Energy Conversion using Novel Composite Materials and Solar Irradiation) and by the Slovenian Research Agency, research core funding No. P1-0134, national project No. L7-1848 and bilateral project BI-HR/18-19-043.

Acknowledgments: The authors acknowledge the Faculty of Chemistry and Chemical Technology of the University of Ljubljana, Ruđer Bošković Institute and the National Institute of Chemistry for the material and equipment support in conducting the research.

Conflicts of Interest: The authors declare no conflict of interest.

References

1. Jafari, T.; Moharreri, E.; Amin, A.S.; Miao, R.; Song, W.; Suib, S.L. Photocatalytic water splitting—the untamed dream: A review of recent advances. *Molecules* **2016**, *21*, 900. [[CrossRef](#)] [[PubMed](#)]
2. Loeb, S.K.; Alvarez, P.J.J.; Brame, J.A.; Cates, E.L.; Choi, W.; Crittenden, J.; Dionysiou, D.D.; Li, Q.; Li-Puma, G.; Quan, X.; et al. The technology horizon for photocatalytic water treatment: Sunrise or sunset? *Environ. Sci. Technol.* **2019**, *53*, 2937–2947. [[CrossRef](#)] [[PubMed](#)]
3. Schneider, J.; Matsuoka, M.; Takeuchi, M.; Zhang, J.; Horiuchi, Y.; Anpo, M.; Bahnemann, D.W. Understanding TiO₂ photocatalysis: Mechanism and materials. *Chem. Rev.* **2014**, *114*, 9919–9986. [[CrossRef](#)] [[PubMed](#)]
4. Bumajdad, A.; Madkour, M. Understanding the superior photocatalytic activity of noble metals modified titania under UV and visible light irradiation. *Phys. Chem. Chem. Phys.* **2014**, *16*, 7146. [[CrossRef](#)]
5. Basavarajappa, P.S.; Patil, S.B.; Ganganagappa, N.; Reddy, K.R.; Raghu, A.V.; Reddy, C.V. Recent progress in metal-doped TiO₂, non-metal doped/codoped TiO₂ and nanostructured hybrids for enhanced photocatalysis. *Int. J. Hydrog. Energy* **2020**, *45*, 7764–7778. [[CrossRef](#)]
6. Ge, J.; Zhang, Y.; Heo, Y.-J.; Park, S.-J. Advanced design and synthesis of composite photocatalysts for the remediation of wastewater: A review. *Catalysts* **2019**, *9*, 122. [[CrossRef](#)]
7. Humayun, M.; Raziq, F.; Luo, W. Modification strategies of TiO₂ for potential applications in photocatalysis: A critical review. *Green Chem. Lett. Rev.* **2018**, *11*, 86–201. [[CrossRef](#)]
8. Žerjav, G.; Arshad, M.S.; Djinović, P.; Junkar, I.; Kovač, J.; Zavašnik, J.; Pintar, A. Improved electron-hole separation and migration in anatase TiO₂ nanorod/reduced graphene oxide composites and their influence on photocatalytic performance. *Nanoscale* **2017**, *9*, 4578. [[CrossRef](#)]
9. Minella, M.; Sordello, F.; Minero, C. Photocatalytic process in TiO₂/graphene hybrid materials. Evidence of charge separation by electron transfer from reduced graphene oxide to TiO₂. *Catal. Today* **2017**, *281*, 29–37. [[CrossRef](#)]
10. Park, S.; An, J.; Potts, J.R.; Velamakanni, A.; Murali, S.; Ruoff, R.S. Hydrazine-reduction of graphite- and graphene oxide. *Carbon* **2011**, *49*, 3019–3023. [[CrossRef](#)]
11. Sykam, N.; Madhavi, V.; Rao, G.M. Rapid and efficient green reduction of graphene oxide for outstanding supercapacitors and dye adsorption applications. *J. Environ. Chem. Eng.* **2018**, *6*, 3223–3232. [[CrossRef](#)]
12. Giovanetti, R.; Rommozzi, E.; Zannotti, M.; D’Amato, C.A. Recent advances in graphene based TiO₂ nanocomposites (GTiO₂Ns) for Photocatalytic Degradation of Synthetic Dyes. *Catalysts* **2017**, *7*, 305. [[CrossRef](#)]
13. Kong, D.; Zhao, M.; Li, S.; Huang, F.; Song, J.; Yuan, Y.; Shen, Y.; Xie, A. Synthesis of TiO₂/rGO Nanocomposites with Enhanced Photoelectrochemical Performance and Photocatalytic Activity. *Nano* **2015**, *11*, 1650007. [[CrossRef](#)]
14. Nainani, R.K.; Thakur, P. Facile synthesis of TiO₂-RGO composite with enhanced performance for the photocatalytic mineralization of organic pollutants. *Water. Sci. Technol.* **2016**, *73*, 1927–1936. [[CrossRef](#)] [[PubMed](#)]
15. Aqeel, M.S.; Imran, M.; Ikram, M.; Majeed, H.; Naz, M.; Ali, S.; Ahmad, M.A. TiO₂@RGO (reduced graphene oxide) doped nanoparticles demonstrated improved photocatalytic activity. *Mater. Res. Express* **2019**, *6*, 086215. [[CrossRef](#)]
16. Tajammul Hussain, S.; Khan, K.; Hussain, R. Size control synthesis of sulfur doped titanium dioxide (anatase) nanoparticles, its optical property and its photo catalytic reactivity for CO₂ + H₂O conversion and phenol degradation. *J. Nat. Gas Chem.* **2009**, *18*, 383–391. [[CrossRef](#)]
17. Yu, J.; Liu, S.; Xiu, Z.; Yu, W.; Feng, G. Synthesis of sulfur-doped TiO₂ by solvothermal method and its visible-light photocatalytic activity. *J. Colloid Interface Sci.* **2009**, *471*, L23–L25. [[CrossRef](#)]
18. Liu, G.; Sun, C.; Smith, S.C.; Wang, L.; Qing, G.L.; Cheng, H.-M. Sulfur doped anatase TiO₂ single crystals with a high percentage of {0 0 1} facets. *J. Colloid Interface Sci.* **2010**, *349*, 477–483. [[CrossRef](#)]
19. Nam, S.-H.; Kim, T.K.; Boo, J.-H. Physical property and photo-catalytic activity of sulfur doped TiO₂ catalysts responding to visible light. *Catal. Today* **2012**, *185*, 259–262. [[CrossRef](#)]
20. Gomathi Devi, L.; Kavitha, R. Enhanced photocatalytic activity of sulfur doped TiO₂ for the decomposition of phenol: A new insight into the bulk and surface modification. *Mater. Chem. Phys.* **2014**, *143*, 1300–1308. [[CrossRef](#)]
21. Hummers, W.S.; Offeman, R.E. Preparation of graphitic oxide. *J. Am. Chem. Soc.* **1958**, *80*, 1339. [[CrossRef](#)]

22. Kete, M.; Pavlica, E.; Fresno, F.G.; Bratina, U. Lavrencic Stangar, Highly active photocatalytic coatings prepared by a low-temperature method. *Environ. Sci. Pollut. Res.* **2014**, *21*, 11238–11249. [[CrossRef](#)] [[PubMed](#)]
23. Patterson, A.L. The Scherrer formula for X-ray particle size determination. *Phys. Rev.* **1939**, *56*, 978–982. [[CrossRef](#)]
24. Moghaddam, H.M.; Nasirian, S. Dependence of activation energy and lattice strain on TiO₂ nanoparticles? *Nanosci. Methods* **2012**, *1*, 201–212. [[CrossRef](#)]
25. López, R.; Gómez, R. Band-gap energy estimation from diffuse reflectance measurements on sol-gel and commercial TiO₂: A comparative study. *J. Sol-Gel Sci. Technol.* **2012**, *61*, 1–7. [[CrossRef](#)]
26. Radón, A.; Włodarczyk, P.; Łukowiec, D. Structure, temperature and frequency dependent electrical conductivity of oxidized and reduced electrochemically exfoliated graphite. *Phys. E* **2018**, *99*, 82–90. [[CrossRef](#)]
27. Kudin, K.N.; Ozbas, B.; Schniepp, H.C.; Prud'homme, R.K.; Aksay, I.A.; Car, R. Raman spectra of graphite oxide and functionalized graphene sheets. *Nano Lett.* **2008**, *8*, 36–41. [[CrossRef](#)]
28. Suave, J.; Amorim, S.M.; Ângelo, J.; Andrade, L.; Mendes, A.; Moreira, R.F.P.M. TiO₂/reduced graphene oxide composites for photocatalytic degradation in aqueous and gaseous medium. *J. Photochem. Photobiol. A* **2017**, *348*, 326–336. [[CrossRef](#)]
29. Cravanzola, S.; Cesano, F.; Gaziano, F.; Scarano, D. Sulfur-doped TiO₂: Structure and surface properties. *Catalysts* **2017**, *7*, 214. [[CrossRef](#)]
30. Lin, H.; Huang, C.P.; Li, W.; Ni, C.; Ismat Shah, S.; Tseng, Y.-H. Size dependency of nanocrystalline TiO₂ on its optical property and photocatalytic reactivity exemplified by 2-chlorophenol. *Appl. Catal. B* **2006**, *68*, 1–11. [[CrossRef](#)]
31. Liu, Y. Hydrothermal synthesis of TiO₂-RGO composites and their improved photocatalytic activity in visible light. *RSC Adv.* **2014**, *4*, 36040. [[CrossRef](#)]
32. Pallotti, D.K.; Passoni, L.; Maddalena, P.; Di Fonzo, F.; Lettieri, S. Photoluminescence mechanisms in anatase and rutile TiO₂. *J. Phys. Chem. C* **2017**, *121*, 9011–9021. [[CrossRef](#)]
33. Liu, Q.-L.; Zhao, Z.-Y.; Liu, Q.-J. Analysis of sulfur modification mechanism for anatase and rutile TiO₂ by different doping modes based on GGA + U calculation. *RSC Adv.* **2014**, *4*, 32100–32107. [[CrossRef](#)]
34. Kovacic, M.; Kusic, H.; Fanetti, M.; Lavrencic Stangar, U.; Valant, M.; Dionysiou, D.D.; Loncaric Bozic, A. TiO₂-SnS₂ nanocomposites: Solar-active photocatalytic materials for water treatment. *Environ. Sci. Pollut. Res.* **2017**, *24*, 19965–19979. [[CrossRef](#)] [[PubMed](#)]
35. Rajagopal, R.; Ryu, K.-S. Synthesis of rGO-doped Nb₄O₅-TiO₂ nanorods for photocatalytic and electrochemical storage applications. *Appl. Catal. B* **2018**, *236*, 125–139. [[CrossRef](#)]
36. Kusiak-Nejman, E.; Wanag, A.; Kapica-Kozar, J.; Kowalczyk, Ł.; Zgrzebnicki, M.; Tryba, B.; Przepiórski, J.; Morawski, A.W. Methylene blue decomposition on TiO₂/reduced graphene oxide hybrid photocatalysts obtained by a two-step hydrothermal and calcination synthesis. *Catal. Today* **2019**, in press. [[CrossRef](#)]
37. Wang, W.; Wang, Z.; Liu, J.; Luo, Z.; Suib, S.L.; He, P.; Ding, G.; Zhang, Z.; Sun, L. Single step one-pot synthesis of TiO₅ nanosheets doped with sulfur on reduced graphene oxide with enhanced photocatalytic activity. *Sci. Rep.* **2017**, *7*, 46610. [[CrossRef](#)]
38. Kovacic, M.; Katic, J.; Kusic, H.; Loncaric Bozic, A.; Metikos Hukovic, M. Elucidating the photocatalytic behavior of TiO₂-SnS₂ composites based on their energy band structure (Supplementary). *Materials* **2018**, *11*, 1041. [[CrossRef](#)]
39. Zhang, Y.C.; Li, J.; Xu, H.Y. One-step in situ solvothermal synthesis of SnS₂/TiO₂ nanocomposites with high performance in visible light-driven photocatalytic reduction of aqueous Cr(VI). *Appl. Catal. B* **2012**, *123–124*, 18–26. [[CrossRef](#)]
40. Alazmi, A.; El Tall, O.; Rasul, S.; Hedhili, M.N.; Patole, S.P.; Costa, P.M.F.J. A process to enhance the specific surface area and capacitance of hydrothermally reduced graphene oxide. *Nanoscale* **2016**, *8*, 17782–17787. [[CrossRef](#)]

41. Tayel, A.; Ramadan, A.R.; El Seoud, O.A. Titanium dioxide/graphene and titanium dioxide/graphene oxide nanocomposites: Synthesis, characterization and photocatalytic applications for water decontamination. *Catalysts* **2018**, *8*, 491. [[CrossRef](#)]
42. Orth, E.S.; Ferreira, J.G.L.; Fonsaca, J.E.S.; Blaskiewicz, S.F.; Domingues, S.H.; Dasgupta, A.; Terrones, M.; Zarbin, A.J.G. pK_a determination of graphene-like materials: Validating chemical functionalization. *J. Colloid Interface Sci.* **2016**, *467*, 239–244. [[CrossRef](#)] [[PubMed](#)]



© 2020 by the authors. Licensee MDPI, Basel, Switzerland. This article is an open access article distributed under the terms and conditions of the Creative Commons Attribution (CC BY) license (<http://creativecommons.org/licenses/by/4.0/>).